REDESIGN OF THE LAST TWO STAGES OF A MECHANICAL DRIVE STEAM TURBINE

by
David A. Henry
Rotating Equipment Engineer
Amoco Petroleum Products
Texas City, Texas
Paul E. DiCristoforo
Senior Design Engineer
TurboCare
Chicopee, Massachusetts
Timothy J. Ewer
Senior Development Engineer
and
Michael Mindock
Manager, Compressor Engineering
Demag DeLaval Turbomachinery Corp.
Trenton, New Jersey

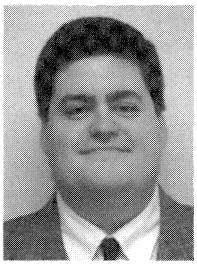

David A. Henry is a Rotating Equipment Engineer with Amoco Petroleum Products at the Texas City, Texas refinery. He has worked at Amoco for eight years in various project and maintenance positions. Mr. Henry's current responsibilities are to provide technical support to operations and maintenance for rotating equipment. This includes rotating equipment vibration monitoring, troubleshooting, performance testing, and optimization. He is responsible for designing and implementing reliability improvements and developing long term maintenance strategies for major pieces of rotating equipment.

Mr. Henry has a B.S. degree in Mechanical Engineering from Louisiana Tech University (1990). He is a member of ASME.

Paul E. DiCristoforo is a Senior Design Engineer at TurboCare Headquarters in Chicopee, Massachusetts. He has worked at TurboCare on large scale steam turbine redesigns and various gas turbine blade projects for the past two years. Prior to this, he was employed by GE for 11 years in various locations as a Marine Field Engineer, an After Market Design Engineer on small and medium steam turbines, a Rotor Design and Development Engineer for gas turbines, and a Hot Gas Path Design Engineer for gas turbines.

Mr. DiCristoforo has a B.S. degree in Mechanical Engineering from the University of Massachusetts at Amherst (1985) and is a member of ASME.

Timothy J. (Tim) Ewer is a Senior Development Engineer at Demag Delaval Turbomachinery, in Trenton, New Jersey. He has been with Delaval for the past 18 years as a Solid Mechanics Engineer in the R&D Department. The first 10 years of that time were devoted to work on submarine main condenser design for the Delaval Condenser Division. The past eight years' work has focused on steam turbines, more specifically, on turbine component standardization and blade design and analysis.

Mr. Ewer received his B.S. degree in Mechanical Engineering from Brooklyn Polytechnic.

ABSTRACT

A six stage mechanical drive steam turbine rated at 13,300 hp was installed at a petroleum facility in Texas to drive a multistage centrifugal compressor used in recycle gas service on a high pressure hydrogen cracker. Since its installation, there has been a failure of either the fifth or sixth stage blades at intervals of 18 months to two years. The blades failed due to high cycle fatigue initiating in the dovetail root attachment.

To alleviate this problem, wider, more robust blades with improved aerodynamics were designed, which include Z-shrouds and a new root dovetail attachment with a lower stress concentration.

INTRODUCTION

The steam turbine was installed in 1985, at the Amoco Petroleum Products, Texas City, Texas, facility. This turbine had a history of fifth and sixth stage blades breaking, due to fatigue, causing high vibration and forcing a unit shutdown. The fifth and sixth stage blades were originally free standing blades with no

lashing wires or bands. In order to prevent further failures, new blades were designed that were resistant to fatigue, even if they ran on resonance. A photograph comparing the original and redesigned blades is shown in Figures 1 and 2. The installation of wider blades required the removal of the existing wheels and the addition of wider wheels by weld buildup. A comparison of the original and redesigned rotor is shown in Figures 3 and 4. The constraints of the existing envelope required machining of the casing and diaphragms, and the replacement of stationary hardware in the region of the blade tips. In addition, the sixth stage blade experienced severe erosion in the leading edge at the tip, the sixth stage diaphragm experienced erosion in the leading edge, and the fifth stage blade also experienced erosion, although it was less severe (Figure 5).

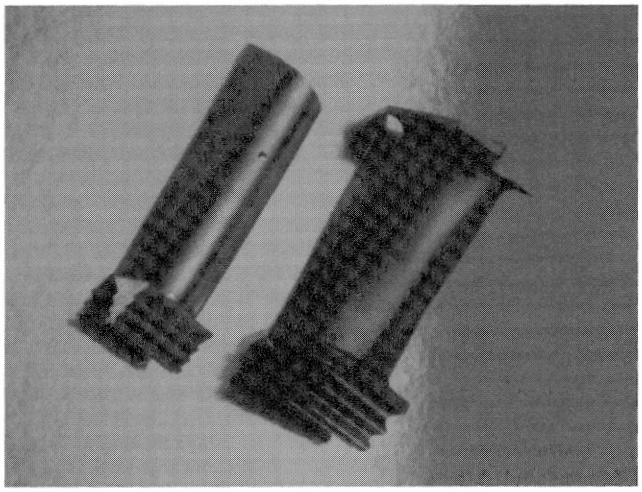

Figure 1. Comparison of Original and Redesigned Stage Five Blades.

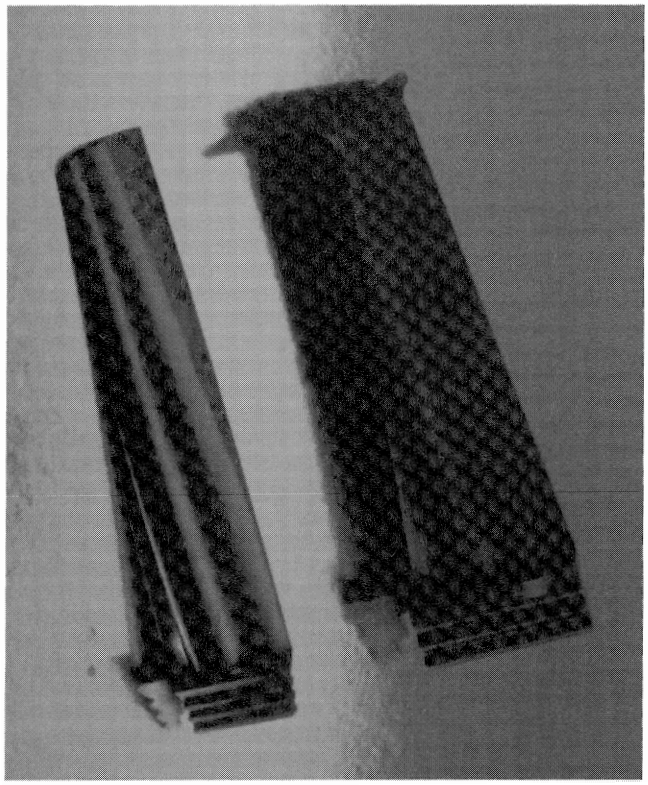

Figure 2. Comparison of Original and Redesigned Stage Six Blades.

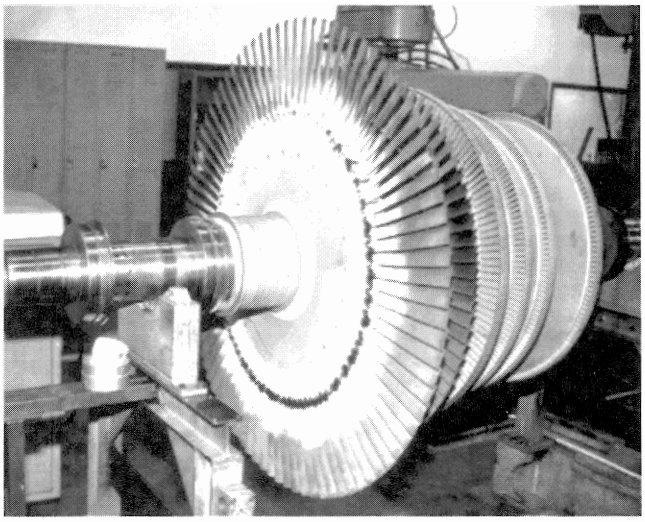

Figure 3. Original Bladed Rotor.

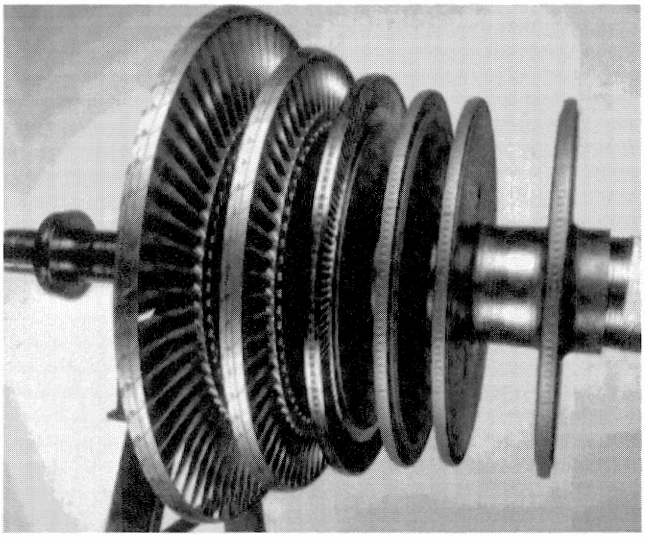

Figure 4. Redesigned Bladed Rotor.

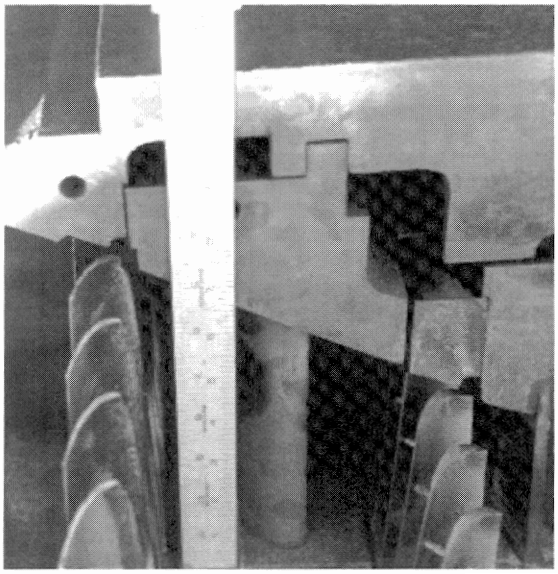

Figure 5. Erosion in Fifth Stage Blade and Sixth Stage Blade and Partition.

OPERATIONAL HISTORY

The first blade failure occurred in May 1992, on a fifth stage blade. Another failure occurred in October 1992. These blades were broken at the top hook in the fir tree root. Metallurgical examination revealed the crack was caused by fatigue. At that time, extensive analysis by consultants revealed a resonant frequency present at 6730 Hz. A nozzle passing frequency (NPF) of 6750 Hz at 8100 rpm appeared to be exciting the resonant frequency. This additional alternating stress due to vibration occurred at the same location as the maximum continuous stress due to centrifugal force. This caused localized overstressing, leading to a fatigue crack. The analysis also revealed that the sixth stage blades (identical in air foil shape, but longer than fifth stage) had a higher static stress level due to centrifugal force (as expected) and also had resonant frequencies present in the NPF operating range (6340 Hz and 6530 Hz). However, the peak stresses due to these resonant frequencies were low and were not at the same location as the static stress.

Steam conditions were also investigated and found to be different from design. The steam turbine was operated with a higher inlet pressure (450 psig versus 390 psig), lower inlet temperature (600°F versus 650°F), and a better vacuum (27 to 28 in hg versus 25 in hg). These conditions also increased the stresses on the blading due to steam bending loads.

The fifth stage blade design was examined to determine possible changes to eliminate the resonant frequency from the NPF operating speed range. After many designs were considered, a modification was implemented in November 1992. These design modifications changed the resonant frequencies to 5610 Hz and 8690 Hz, outside the NPF operating speed range. The modifications entailed adding a straight lashing wire (seven blades per group), and a zigzag block and lashing wire between each blade. In addition, crush pins were added underneath each blade root to prestress the blade fir tree in the disk. Rivets were added between each blade at the top of the fir tree to lock the blades into the axial entry fir tree. The original design had rivets located between every other blade, and no crush pins. All of these modifications were designed and manufactured by a second party supplier.

In January 1996, a sixth stage blade failure occurred for the first time. Examination of the failed blades indicated that several fifth stage zigzag pins had come loose and impacted the leading edge of the sixth stage blades. Fatigue cracks then initiated at the stress risers, caused by the impact damage. The blades were breaking approximately one-third of the way up the length of the blade. The spare rotor was installed and another investigation begun on the sixth stage blades. Outside companies were brought in to examine the blade design again and propose solutions. While this investigation was proceeding, another sixth stage blade failure occurred in November 1996. These blades broke during a probable high condensate level caused by an emergency unit shutdown. Examination revealed a stress riser on the leading edge of the blades and a fatigue crack that was mostly high cycle fatigue, but was accelerated by several low cycle high stress events. Due to time constraints, 10 blades in the sixth stage were replaced during the shutdown and the turbine was placed back into service. The investigation was completed and it was decided to proceed with modifying the spare rotor to the new design.

In December 1996, another sixth stage blade failure occurred. Due to time constraints, and the long lead time to procure additional blades for the sixth stage, a decision was made to temporarily downgrade the turbine horsepower output by removing the sixth stage blades. This caused a loss of approximately 3000 hp.

BLADE REDESIGN

Preliminary Design

Based on the operational experience, it was clear that a more robust design was needed. Given the variable speed operating history, operation on resonance during some periods is a given. The failure mechanism is high cycle fatigue initiating in a stress concentrator in the root attachment. A blade resonance had to be present for some time during the operating cycle to result in alternating stresses, which would cause material fatigue cracking. The original design was susceptible to high cycle fatigue cracking, because there were high stress concentrations in the root dovetail attachment, due to very small fillet radii. It was a free standing blade that was very responsive to resonances, and it was a narrow airfoil that resulted in high steady bending stresses in the blade.

If there is a blade resonance, high cycle fatigue cracks will initiate if the blade vibratory stresses in the resonant mode are higher than the fatigue strength of the material. At resonance, the vibratory stress is proportional to the stimulus on the blade, and inversely proportional to the damping of the blade:

$$\text{Vibratory Stress} = f\frac{\text{Stimulus} \times \text{RRF}}{\text{Damping}} \qquad (1)$$

Where:

Stimulus = Alternating force on the blade expressed as a percent of the blade steady load

Damping = Logarithmic decrement damping due to material damping and coulomb friction at the blade attachment and shroud (if included in the design). As can be seen from Equation (1), the vibratory stress (or response) is inversely proportional to damping.

RRF = Resonant response factor, or the attenuation in response due to the phase relationship between the stimulus and the particular mode shape

The blades were redesigned to be tolerant to operation on resonance. This was achieved by applying the following features:

- Z-shrouded blades with continuous coupling to dramatically suppress the response of the potentially resonant modes of vibration, when compared with the original blades
- Blades with a larger section modulus in the airfoil root to reduce the root steam bending stress
- Root attachments with larger fillet radii and, hence, a lower stress concentration
- Harmonic tuning of the diaphragm to reduce the stimulus on the blade, if resonance occurs
- Wider wheels and thinner diaphragms to accommodate the wider, more robust blades

The last two stages of a standard back end that met all of our requirements and were near to the required airfoil height were chosen. They were then scaled in all dimensions to the proper height for this application. After scaling, a larger, standard root attachment was selected that provided acceptable stress levels for blades of this size. Based on preliminary calculations, considering the effect of the features noted above, the vibratory stresses will be reduced by a factor of 52 to one for the L-1 stage and a factor of 26 to one for the L-0 stage. However, the blades were no longer a standard design and would require a thorough aerodynamic and mechanical evaluation.

Aerodynamic Design

A two-dimensional, row-by-row, through flow code incorporating an empirical loss model, verified with inhouse test data, was used to analyze the aerodynamic performance of the original two-stage low pressure (LP) -end (Steltz, 1990). The results of this analysis clearly indicated that the original LP-end was not achieving good efficiency and mechanical reliability, because the blading was operating with very high incidence.

Airfoil incidence is defined as the airfoil inlet angle, minus the fluid angle, measured from the tangential plane. Minimum airfoil

loss occurs at near zero incidence (≈ −2 to −5 degrees due to circulation), and as incidence increases, the efficiency of the thermal-to-kinetic energy conversion decreases, resulting in reduced power output. The incidence profile for the L-1 rotor blade, L-0 stator vane, and L-0 rotor blade is illustrated in Figure 6. (The incidence profile of the L-1 stator vane was not computed, since the last rateau stage was not analyzed.) As is evident from Figure 6, the original design operates with very high incidence. This is especially noticeable for the L-0 rotor blade, which has −12 degree incidence at the hub, increasing to −81 degree incidence at the tip.

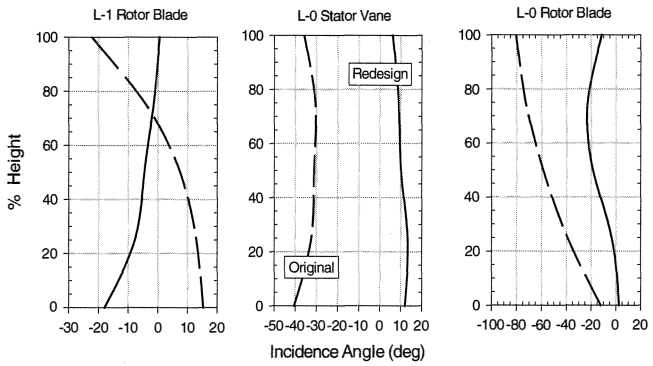

Figure 6. Incidence Profile for L-1 Rotor Blade, L-0 Stator Vane, and L-0 Rotor Blade.

In the two-phase flow found in a condensing turbine LP-end, incidence not only imposes a thermodynamic performance penalty, it also imposes a mechanical penalty. Water droplets shedding from the stator vane travel more slowly than the fluid, and hence, impact the rotor blade leading edge with greater negative incidence. Therefore, for the original L-0 rotor blade tip, water droplets impact the leading edge approximately normal to the suction surface, producing maximum impact pressure opposite the direction of rotation—the cause of the severe erosion (Krzyzanowski, et al., 1971).

A similar analysis was conducted for the redesigned flowpath, consisting of the original stator vanes and new rotor blades. A substantially better aerodynamic matching was predicted with significantly improved incidence. The incidence profiles for the redesign is over-plotted in Figure 6. The reduction in the magnitude of incidence for the L-1 rotor blade, L-0 stator vane, and L-0 rotor blade is dramatic. Most successful is the L-0 rotor blade: tip incidence is reduced from −81 degrees to just −12 degrees. And with the reduced incidence at the L-0 rotor tip, erosion should no longer be as severe (Krzyzanowski, et al., 1971). For a comparison of the original and redesigned blade airfoils, refer to Figure 7.

With the improved rotor blade incidence profiles, the rotor blading is better able to transfer the tangential momentum created by the stator vanes to mechanical energy. Consequently, substantially more power output is predicted for both stages of the redesign. Table 1 is a comparison of the original and redesign predicted stage power. The redesign is predicted to produce 37.3 percent greater power in the last two stages than the original design. This provides an approximately 9.5 percent increase in total output.

Mechanical Design

The proposed fix for these stages was a completely new disk and blade. With this radical change and knowing the repetitive nature of the failure history, it was important to understand the stress and vibration characteristics of each new stage. To accomplish this, a finite element analysis (FEA) of each stage was performed.

A key tool in performing this analysis was the finite element code BLADE-ST (an EPRI software product developed by Stress

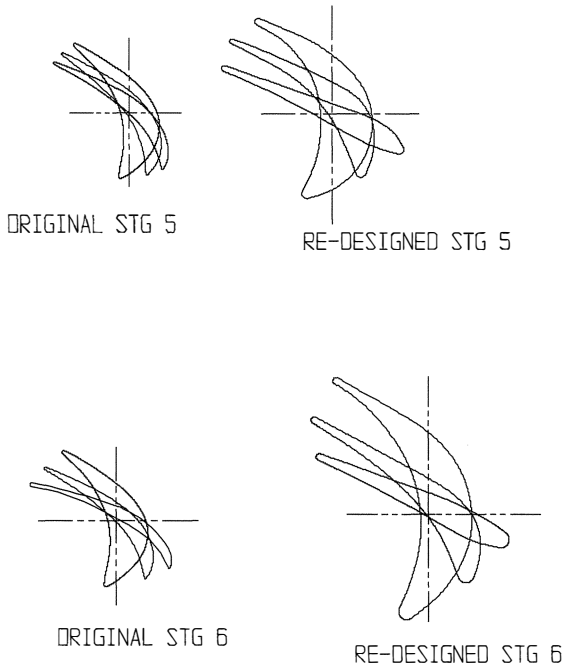

Figure 7. Comparison of Original and Redesigned Blade Airfoils.

Table 1. Predicted LP-End stage Power for Original and Redesign.

L-1 Stage			L-0 Stage		
Original (hp)	Redesign (hp)	%Δ	Original (hp)	Redesign (hp)	%Δ
1839.	2054.	11.7	1575.	2633.	67.2

Technology Incorporated, Rochester, New York). This product is a preprocessor, solution, and postprocessing code written specifically for steam turbine blading. Several input screens are used to define the model geometry and aerodynamic loading. The program will perform the steady stress, modal, and dynamic solutions for many different blade/disk designs (e.g., axial entry, radial entry, grouped, etc.).

For this analysis, a linear elastic FEA model of each stage was constructed. Each model consists of eight node brick elements. The analysis requirements were to determine stresses in the disk fastener, the blade fastener, the airfoil, and the shroud. The loading to be considered was centrifugal plus steam loading. The mode shapes and natural frequencies for each stage were also determined.

The designs analyzed have axial entry fir tree fasteners, taper twisted airfoils, and interconnecting "Z" shaped shrouds (Figure 8).

Each model consisted of a single blade sector, or slice of the wheel. The modelled components are disk, blade fastener, blade platform, airfoil, and shroud. The disk structure has zero displacement at the shaft outer diameter. The blade fastener is fixed to the disk at the contact points by means of coupled node sets. The blade fastener and platform share coincident nodes. The airfoil is joined to the platform and shroud by a combination of coincident nodes and constraint equations.

The appropriate symmetric boundary conditions are applied at the cut tangential faces of the disk and the contacting faces of the shroud. This forces the disk section to behave as a full disk. The same reasoning is applied to the shroud. During operation, one component of the airfoil deformation is an untwisting from its static shape. The shroud is designed to contact the adjacent shroud under this rotation, loading up the contact faces and locking the shrouds together. Therefore, symmetry boundary conditions are also applied here.

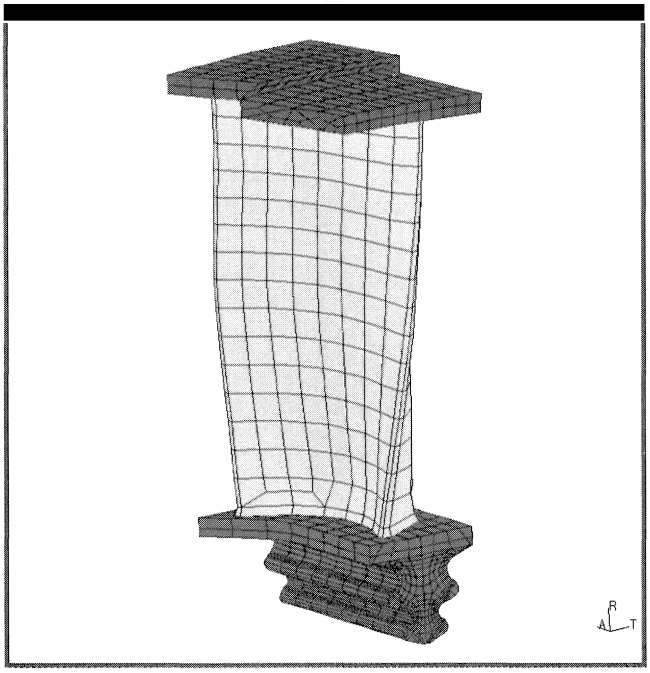

Figure 8. Stage Five "Blade" Model.

Common to all the FEA analyses for these stages is applying the principals of substructuring. The analysis of a structure can be accomplished by the analysis of individual parts of the structure, with the appropriate boundary conditions applied. In the case of a bladed turbine wheel, there is the additional benefit that the whole structure is composed of a single repetitive piece. Therefore, the analysis can be reduced to the solution of the single substructure, a one pitch slice of the wheel.

After completing the input definitions for geometry and loading, the execution of the steady stress analysis is entirely automated by the program. This is also true of the modal analysis. There are some additional inputs related to the modes and frequencies desired, then the program does the rest. It defines the required boundary conditions, selects the master degrees of freedom, and builds the substructure.

Important to predicting the modal response of the system is the proper functioning of the locking shroud design. For easy installation at rest, the shrouds may have some clearance between them. As the rotor speeds up, the blades will twist, and contact will be made between the shrouds. The area and angle of the contact face determines the loads that are generated at speed. The loads should be as high as possible to prevent relative motion between shrouds, but below a predetermined contact stress limit. If insufficient load at speed is calculated, a static load can be introduced by designing the contact face to have an interference at assembly. This is accomplished by taking the finalized shroud design and rotating it in the direction of blade untwist. Building this pretwist into the shroud design will make installation of the blades more difficult, so caution must be exercised. With the shrouds all nested together, the fasteners will no longer be parallel to the disk slots. The additional difficulty introduced is related to the amount of torque that is created as the fasteners are driven into the disk.

A review of the modal solution reveals a graphical representation of the mode shapes for each frequency calculated. The mode shapes can be displayed as either the entire wheel (just the airfoil MDOFs are plotted, Figure 9) or the blades strung out in a straight line. This helps greatly to visualize and identify the modes of vibration. An interference diagram can easily be generated to select modes for dynamic analysis (Figures 10 and 11).

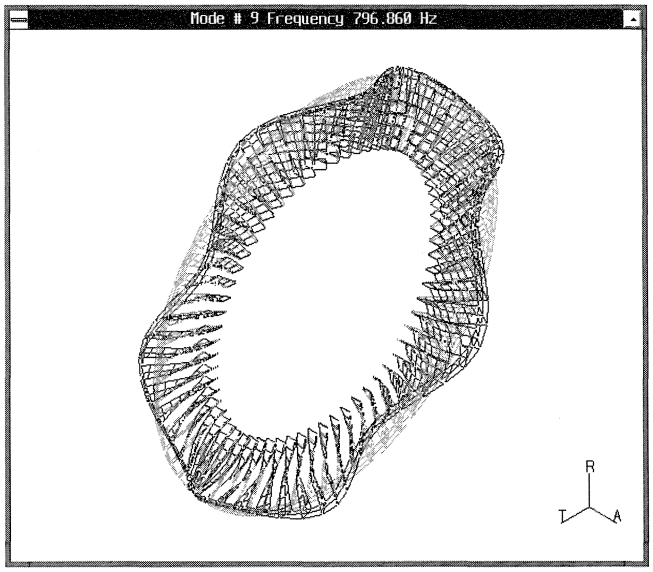

Figure 9. Stage Six Mode Shapes at 797 Hz (6/Rev).

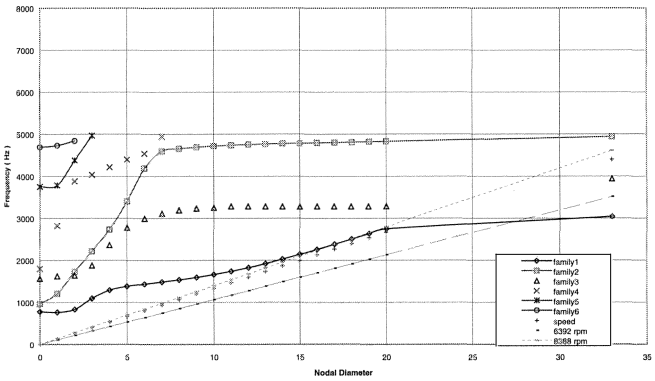

Figure 10. Interference Diagram for Stage Five.

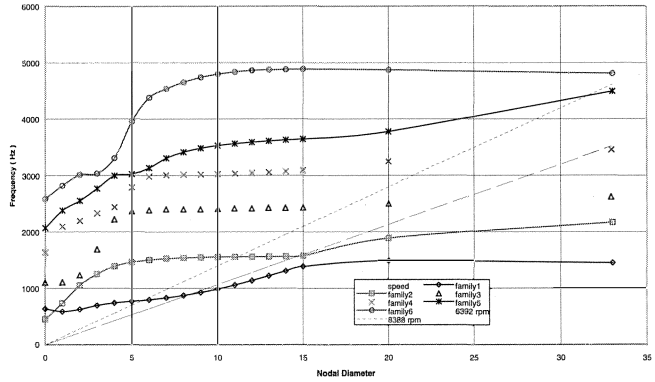

Figure 11. Interference Diagram for Stage Six.

By inspection of the stage five steady stress plot (Figure 12), it can be seen that the average stresses are well within the limits of the titanium blade material, which has a tensile strength of approximately 130 ksi at 200°F. The same is true of the stage six steady stresses, which are plotted in Figure 13.

As can be seen from the interference diagram for stage five (Figure 10), there are no low engine order resonances that are coincident with the operating range of the machine. The calculated frequencies for 14/rev through 20/rev are only slightly above the maximum operating speed of the machine. The unit is not normally run at this speed and these are higher order modes, which are more

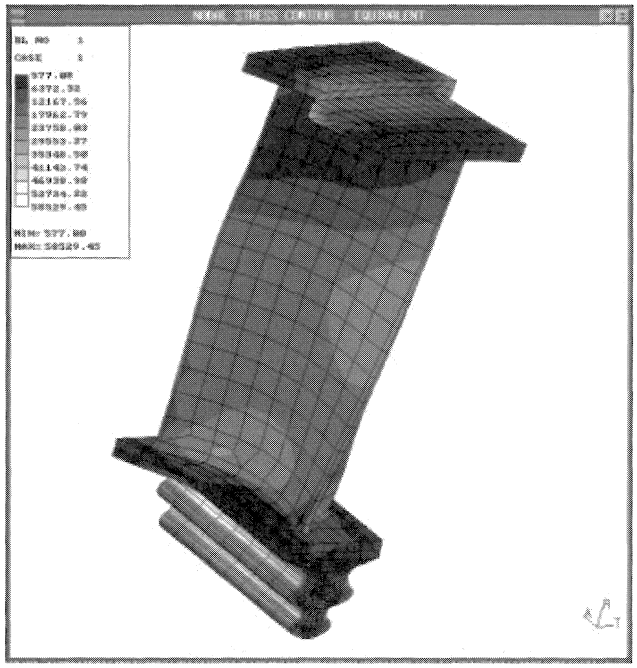

Figure 12. Stage Five Steady Stresses.

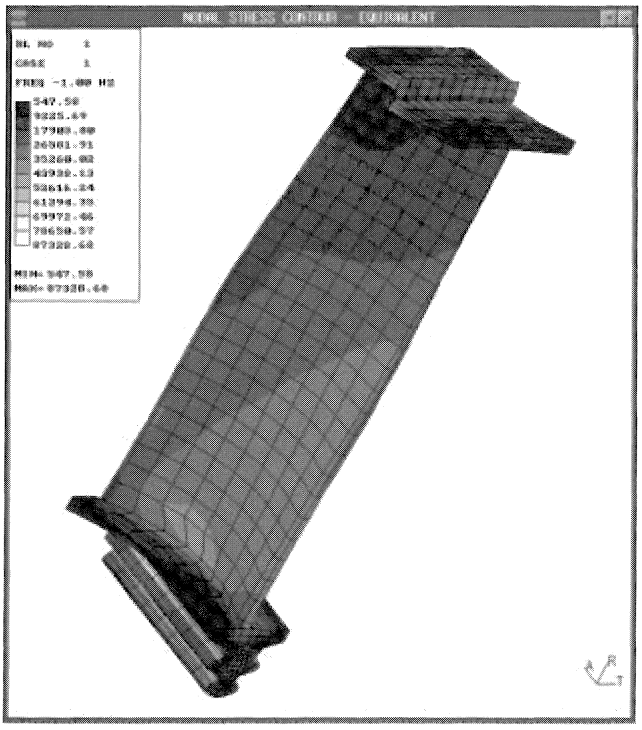

Figure 13. Stage Six Steady Stresses.

difficult to excite. For conservatism, the stimuli for these modes were minimized by harmonic tuning of the diaphragm.

From the interference diagram (Figure 11), it can be seen that the blade will run on resonance on a 6/rev and a 12/rev, at normal operating speed. A forced response was run for both of these modes to determine the vibratory stress levels in the blade. As can be seen in the vibratory stress plot (Figure 14) the vibratory stresses are low for the 6/rev mode. The vibratory stresses in the 12/rev mode (not shown) are even lower. The stimulus for these modes were also minimized by harmonic tuning of the diaphragm. Diaphragm harmonic tuning will be discussed in more detail in a later section.

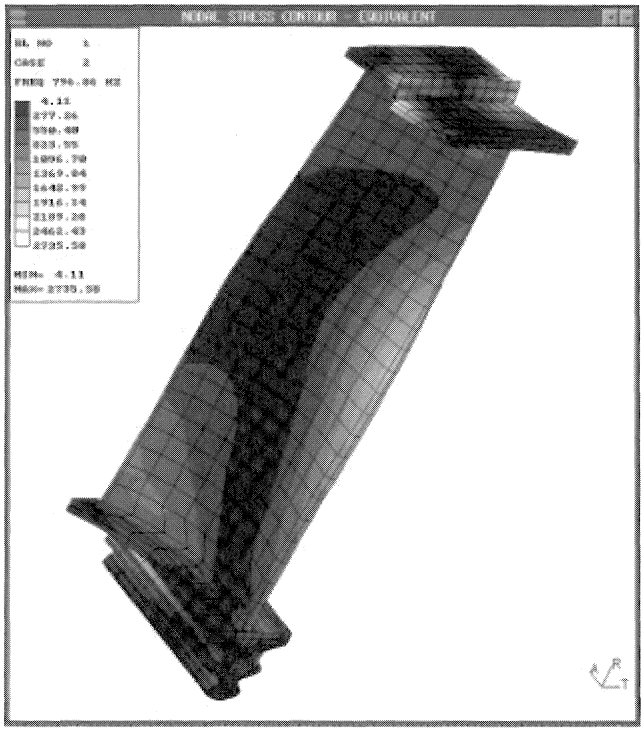

Figure 14. Stage Six Vibratory Stresses for 797 Hz (6/Rev).

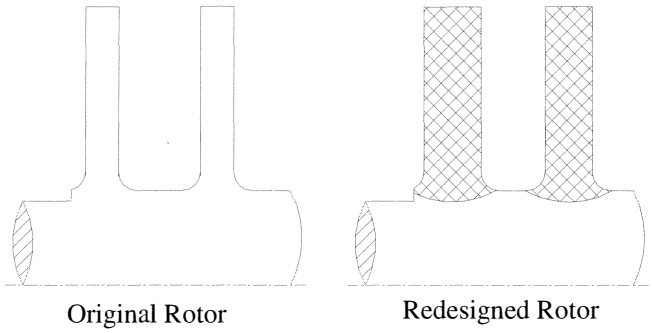

Figure 15. Comparison of Original Rotor to Redesigned Rotor (Crosshatching signifies weld metal).

ROTOR REDESIGN

The new blades are considerably wider than the original design. In order to install them into the existing rotor, wider wheels would be required. This was accomplished by machining the last two stages down to the shaft and producing new, wider wheels by the weld buildup process, as shown in Figure 15.

The welding was performed using the submerged arc welding process. After welding, the welded area was stress relieved and post weld heat treated to achieve the proper material properties. The wheels were inspected by magnetic particle, dye penetrant, and ultrasonic NDT inspection procedures to ensure that there were no defects in the weld metal.

Because the new blades are considerably heavier than the original, the centrifugal load on the wheel will be greater. A two-dimensional axisymmetric finite element analysis was performed on the original design and the new design (Figures 16 and 17) using computerized software. The peak stress is 15 ksi for the original and 20 ksi for the new design. The average Von Mises stress across the wheel is approximately 12 ksi for the original and approximately 16 ksi for the redesign. These stresses are well within allowable limits for the weld material, which has a tensile strength greater than 100 ksi.

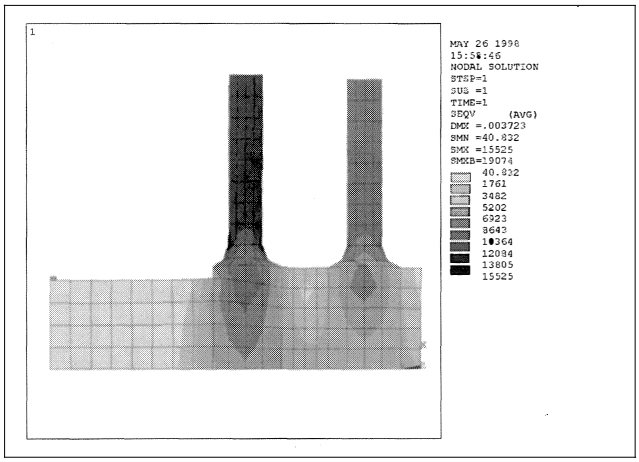

Figure 16. Stresses in Original Rotor.

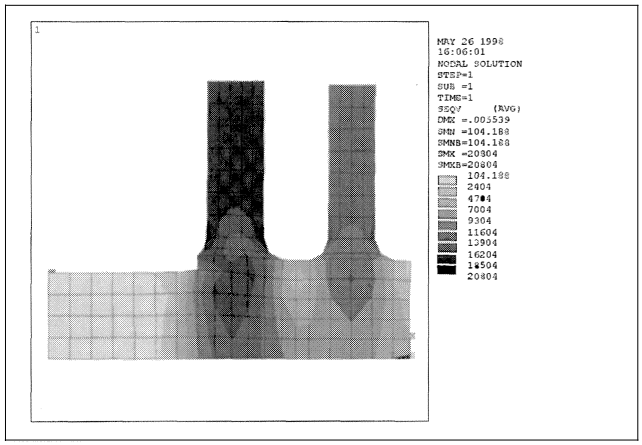

Figure 17. Stresses in Redesigned Rotor.

STATIONARY PART REDESIGN

In order to fit the wider blades and disks into the existing envelope, some modifications to the casing and diaphragms were required.

Casing Redesign

All the changes made to the casing were done strictly to provide proper clearances for the rotor. Figure 18 shows the original cross section on the lower half and the redesign on the upper half, for comparison. Changes were made near the tip of the last stage blade to provide clearance for the integral Z-shroud. A smooth transition from the end of the last stage diaphragm to the exhaust was provided to help minimize water erosion in this area. A step at the aft end of the casing was machined to provide axial clearance for the last stage wheel in the dovetail region. The diaphragm grooves were machined wider, so the diaphragms could be moved axially.

Diaphragm Redesign

The diaphragms are made of cast iron with cast-in airfoils. Since the wider wheels decreased the spacing between wheels, the diaphragms needed to be machined thinner to fit. A finite element analysis using computerized software was performed, assuming worst case stage pressure drops, on the original and redesigned diaphragms for both stages.

The diaphragms were modelled with axisymmetric four-node quad elements for the inner and outer ring, and beam elements to represent the airfoils. As can be seen from the stress plots (Figures 19, 20, 21, and 22), the stresses in these parts are very low and well within allowable limits for cast iron, which has a minimum tensile strength of 20,000 psi.

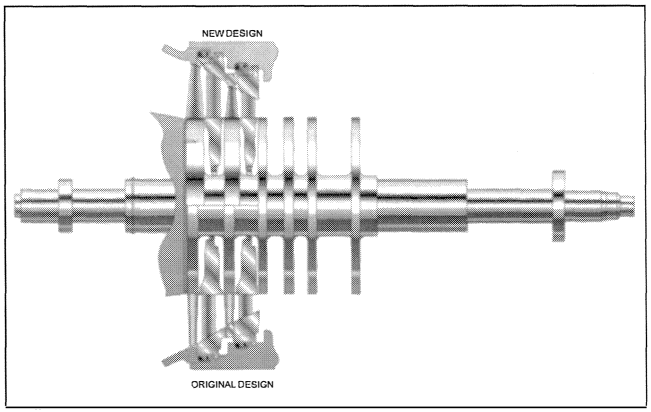

Figure 18. Comparison of Original and Redesign Turbine Cross Section.

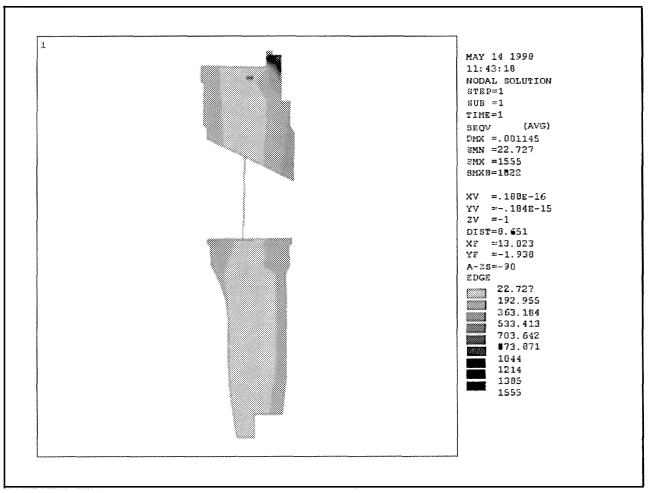

Figure 19. Stage Five Original Diaphragm Stresses.

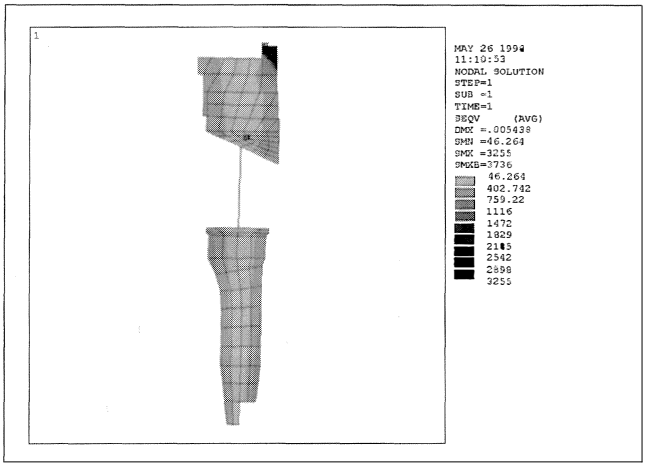

Figure 20. Stage Five Redesign Diaphragm Stresses.

In order to locate the diaphragms in the proper axial location, spacer rings were bolted to the diaphragm steam seal surface and machined to the proper thickness (Figure 23). The grooves in the

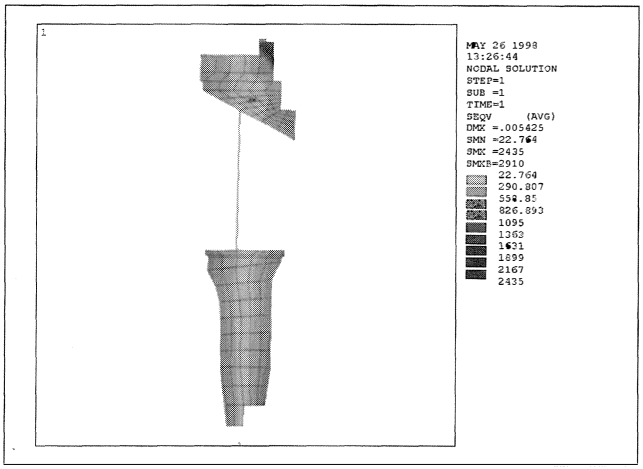

Figure 21. Stage Six Original Diaphragm Stresses.

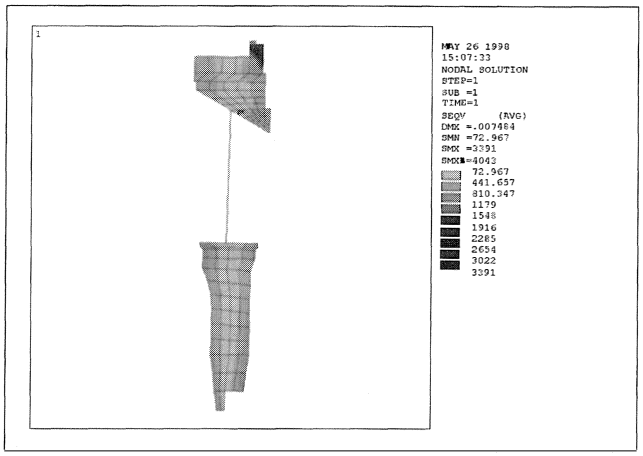

Figure 22. Stage Six Redesign Diaphragm Stresses.

casing had previously been machined to allow for this adjustment. On the L-1 stage, the original moisture ring was redesigned to provide clearance for the blade Z-shroud and to account for the axial relocation of the diaphragm. A filler piece was bolted to the aft end of the L-0 diaphragm to account for the axial relocation (Figure 24).

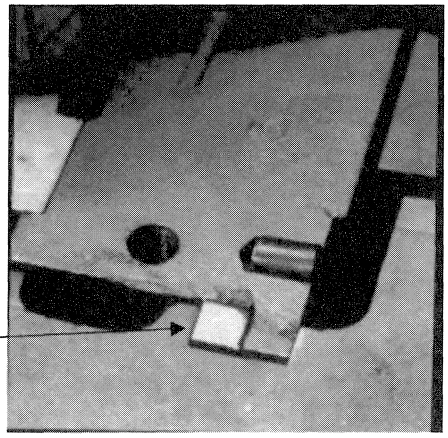

Figure 23. Diaphragm Installed in Casing with Spacer Ring Attached.

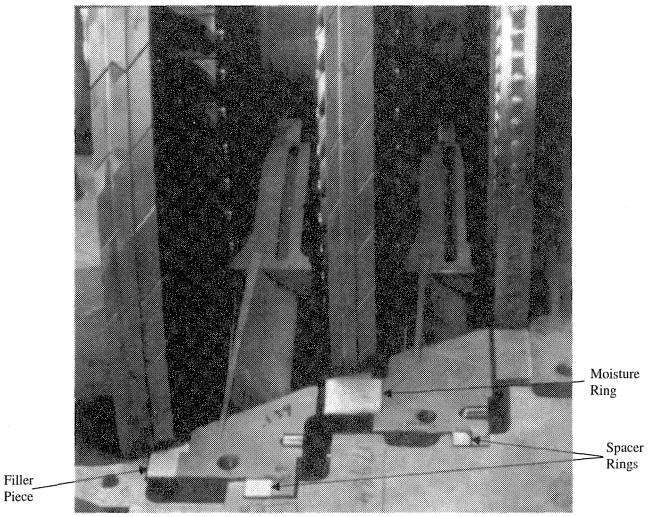

Figure 24. Casing with Rotor and Diaphragms Installed Showing Spacer Rings, Stage Five Moisture Ring, and Stage Six Filler Piece.

Harmonic Tuning

Because of its method of manufacture, a steam turbine diaphragm has variations in the throat and pitch dimensions from one opening to another that will be very small and well within drawing tolerance. These variations will cause flow dissymetries, which, depending upon the pattern, can cause a low harmonic excitation that is coincident with a natural frequency of the downstream rotating blades. If this happens, the blade will run on resonance and, depending on the magnitude of this stimulus, may fail due to high cycle fatigue.

The fifth and sixth stage diaphragms were tuned to minimize the harmonic excitation imposed on the rotating blades using the program MHE (Minimize Harmonic Excitation is a software product of Stress Technologies Incorporated, Rochester, New York). This program performs a fast Fourier transformation on the original nozzle throat/pitch gauging. It then determines which throat openings have the greatest effect on the two harmonics chosen to minimize, and makes adjustments (within limits) to five throats and reevaluates the excitation level. It keeps adjusting five throats at a time until the minimum stimulus level possible is achieved. The harmonic multiples to be minimized are determined based on problem frequencies for the blades. The program only looks at harmonic multiples up to 20. The stimulus is generally low for higher orders. From the interference diagram for stage five (Figure 10), it can be seen that all frequencies are avoided at running speed. The 14th to 20th harmonics of running speed are close to the max continuous running speed, and so the stimulus related to these harmonics have been minimized. The stimuli are reduced below 0.5 percent in all of these instances (Figure 25).

For stage six, the interference diagram (Figure 11) shows that the sixth and 12th nodal diameters are near rated speed. These have been minimized to at or below 0.3 percent, and the sixth harmonic has been reduced by a factor of six to one from the as-found conditions (Figure 26). Should the blades run on resonance, this would greatly reduce the vibratory stress.

STARTUP/OPERATION

The modified rotor was installed during a unit TAR, in early 1998. The case was pulled to allow for the necessary machining to install the modified blading. General repairs were also made to correct for minor case distortions and allow proper diaphragm placement.

Vibration levels after startup were very low (less than 0.75 mil peak-to-peak). The rotor was well balanced and heavily damped when accelerating through the critical speed.

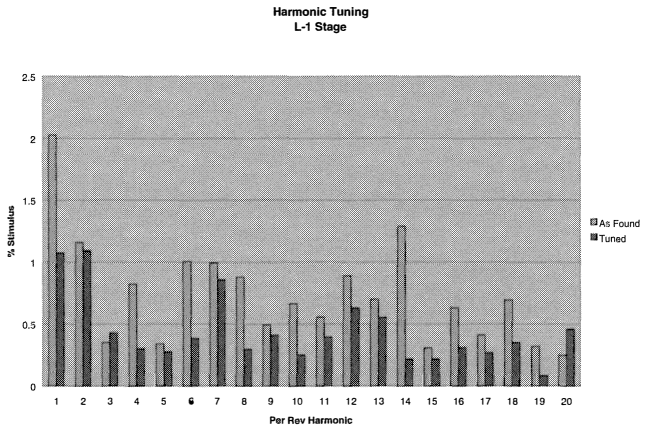

Figure 25. Stage Five Diaphragm Harmonic Tuning Results.

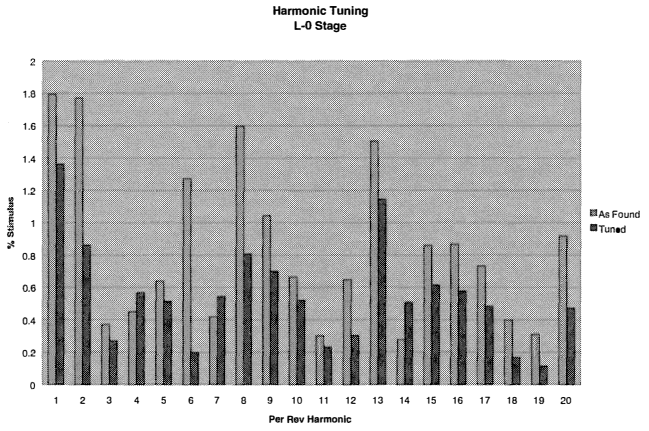

Figure 26. Stage Six Diaphragm Harmonic Tuning Results.

Performance tests were run after startup to see if the extra horsepower of the redesign was measurable. Examination of the data revealed that, in this case, it is very difficult to calculate exact horsepower output of the steam turbine. Since the moisture content of the steam in the condenser cannot be directly measured, the second enthalpy state needed for the efficiency calculation is approximated using the horsepower consumed by the compressor and the steam flowrate. In this case, the compressor driven by the steam turbine is a high pressure hydrogen recycle compressor, with a low delta head and a low temperature rise. The nominal pressures are 1650 psig suction and 2000 psig discharge. The temperatures are 120°F suction and 155°F discharge. The low temperature rise makes the polytropic efficiency very sensitive to any errors in temperature measurement and can affect the specific heat ratio (k) significantly. The nominal compressor efficiency was 75 percent with a gas horsepower of 13,365 hp, but a two to three degree error in the discharge temperature can change that efficiency by ±6 percent. Using the compressor horsepower to determine the steam turbine efficiency gives a nominal steam turbine efficiency of 74 percent ±6 percent. This appears to be slightly lower than the nominal 79 percent efficiency. Several other factors contribute to the perceived lower efficiency. During the time the performance tests were run, the turbine was unable to be run at absolute maximum load due to unit constraints. This led to the steam rack being 85 percent to 90 percent open. Also, the cooling water temperatures were very warm during this time, leading to reduced condenser effectiveness. The condenser vacuum was running at 6 to 7 in hg absolute versus the design conditions of 3 to 4 in hg. This would also affect steam flowrates significantly. Consequently, the absolute horsepower output of the steam turbine cannot be accurately determined at this time.

CONCLUSION

This unit had a long history of failures in its last two stages. By redesigning these stages to stronger blades with increased damping and by tuning the diaphragms, the stresses have been reduced by factors greater than 25:1. The new blades also have a superior aerodynamic design that will result in higher efficiency and reduced water erosion. By welding new disks onto the existing rotor, the repair was done at a fraction of the cost of a new rotor. With the reduction in stress and improved aerodynamics, the blades should not fail, and the unit will be much more reliable and economical.

REFERENCES

Krzyzanowski, J., Weigle, B., and Severin, H., 1971, "Semiempirical Criterion of Erosion Threat in Modern Steam Turbines," ASME Journal of Power Engineering, *1*, pp. 1-6.

Steltz, W., 1990, "A Simplified and Generalized Approach to the Design and Analysis of Axial Flow Steam and Gas Turbine Blade Paths," ASME Advances in Steam Turbine Technology for Power Generation, PWR-*10*, pp. 265-269.